



OPEN

Observation of Dirac state in half-Heusler material YPtBi

M. Mofazzel Hosen¹, Gyanendra Dhakal¹, Klauss Dimitri¹, Hongchul Choi², Firoza Kabir¹, Christopher Sims¹, Orest Pavlosiuk³✉, Piotr Wiśniewski³, Tomasz Durakiewicz^{4,5}, Jian-Xin Zhu^{2,6}, Dariusz Kaczorowski³ & Madhab Neupane¹✉

The prediction of non-trivial topological electronic states in half-Heusler compounds makes these materials good candidates for discovering new physics and devices as half-Heusler phases harbour a variety of electronic ground states, including superconductivity, antiferromagnetism, and heavy-fermion behaviour. Here, we report a systematic studies of electronic properties of a superconducting half-Heusler compound YPtBi, in its normal state, investigated using angle-resolved photoemission spectroscopy. Our data reveal the presence of a Dirac state at the Γ point of the Brillouin zone at 500 meV below the Fermi level. We observe the presence of multiple Fermi surface pockets, including two concentric hexagonal and six half-oval shaped pockets at the Γ and K points of the Brillouin zone, respectively. Furthermore, our measurements show Rashba-split bands and multiple surface states crossing the Fermi level, this is also supported by the first-principles calculations. Our findings of a Dirac state in YPtBi contribute to the establishing of half-Heusler compounds as a potential platform for novel topological phases.

Topological quantum materials with non-trivial electronic band structures have gained intense research interest due to the possibility of exploiting exotic new physics such as Majorana fermions and the quantum spin Hall effect, as well as for their broad potential applications in quantum computing and spintronics^{1–3}. These further lead to the realization and discovery of numerous topologically non-trivial states such as topological insulators (TI), topological Kondo insulators, topological crystalline insulators and topological semimetals, in various material families^{4–17}. Interestingly, ternary half-Heusler compounds have been theoretically predicted to provide a platform for realizing non-trivial states in their electronic structure as a result of their innate characteristic to obtain optimized parameters of topological order and topological phase transitions via tunable band gap and diverse spin-orbit coupling (SOC)^{18–22}. Furthermore, the half-Heusler compounds containing lanthanide elements with strongly correlated *f*-electrons already have various ground states such as antiferromagnetism and superconductivity^{23,24}. Therefore, the presence of *f*-electrons in these systems makes them promising platforms to study the correlated phenomena.

Despite the fact that a decade has already passed since the theoretical prediction of topologically non-trivial states in half-Heusler compounds, there are only a few experimental studies reporting evidences of such states^{25–27}. Large and negative longitudinal magnetoresistance has been reported as a signature of the chiral magnetic anomaly in GdPtBi²⁵. Recent angle-resolved photoemission spectroscopy (ARPES) studies of LnPtBi (Ln = Lu, Y)²⁶ and LuPtSb²⁷ have reported the observations of topological surface states. However, the assignment of topological surface state, as well as proposed origin of those states do not agree with each other. In contrast to those two reports, another ARPES study of several half-Heusler phases LnPtBi (Ln = Lu, Dy, Gd)²⁸ has not found direct evidence of topologically non-trivial electronic states in these materials. Therefore, it is important to undertake new research efforts in order to conclude the nature of electronic structure of half-Heusler phases.

In this work, we report the detailed electronic structure study of YPtBi using ARPES and first-principles calculations. Our systematic study of electronic structure reveals the hexagonal Fermi surface along with the presence of multiple Fermi pockets. Particularly, we find multiple Fermi surface pockets such as hexagonal and oval pockets around the zone centre and the K points of the Brillouin zone (BZ), respectively. Interestingly, our

¹Department of Physics, University of Central Florida, Orlando, FL 32816, USA. ²Theoretical Division, Los Alamos National Laboratory, Los Alamos, NM 87545, USA. ³Institute of Low Temperature and Structure Research, Polish Academy of Sciences, 50-950 Wrocław, Poland. ⁴Idaho National Laboratory, Idaho Falls, ID 83415, USA. ⁵Institute of Physics, Maria Curie - Skłodowska University, 20-031 Lublin, Poland. ⁶Center for Integrated Nanotechnologies, Los Alamos National Laboratory, Los Alamos, NM 87545, USA. ✉email: o.pavlosiuk@intibs.pl; Madhab.Neupane@ucf.edu

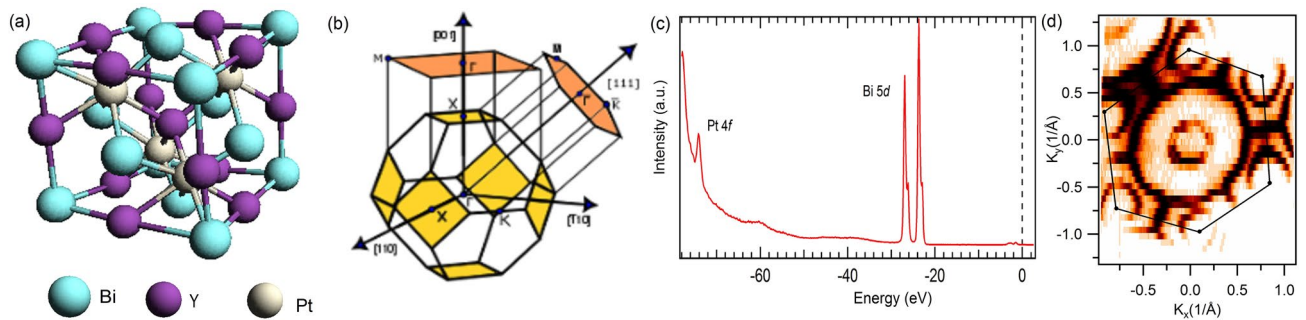


Figure 1. Crystal structure and sample characterization of YPtBi. **(a)** The unit cell of YPtBi compound. **(b)** The bulk Brillouin zone with surface projections along the [001] and [111] directions. High symmetry points are marked in the plot. **(c)** Core level photoemission spectrum. Sharp peaks of Pt 4f and Bi 5d are observed. **(d)** Spectroscopically measured Fermi surface of YPtBi. Black hexagon represents the first Brillouin zone. Observation of hexagonal Brillouin zone confirms that the cleavage plane of the crystal is (111).

data reveal a Dirac state at the Γ point of the BZ where the Dirac point lies at 500 meV below the Fermi level, which is further supported by our first-principles calculations. Moreover, we report Rashba-splitting in the vicinity of the Fermi surface at the M point of the BZ. We also report the presence of multiple surface states in this system. Our findings bolster the evidence for the existence of exotic states within the half-Heusler family. Furthermore, observation of topologically non-trivial electronic states together with the previously reported superconductivity in YPtBi^{29–32}, makes this material a possible platform for further investigations of coexistence of these two phenomena.

Results

Half-Heusler ternary compounds crystallize with space group $F\bar{4}3m$ lacking inversion symmetry³³. Figure 1a shows the unit cell of YPtBi. The sample normally cleaves along either the (111) or (001) plane. Figure 1b shows the schematic bulk BZ with surface projections on the (001) and (111) planes. High symmetry points are also marked in the figure, where Γ is the centre of the BZ, K is defined as the each corner of hexagon and M is the midpoint of two successive corner points. Figure 1c represents the spectroscopic core level measurement of YPtBi with sharp peaks of Bi 5d and Pt 4f at around 26.9 eV and 74 eV, respectively. This confirms that the sample of high quality was used for our measurements. Furthermore, larger spectral weight of Bi 5d indicates the Bi termination. An ARPES measured hexagonal-shaped Fermi surface of YPtBi is shown in Fig. 1d which further confirms that the cleavage plane of the crystal is (111). The slight distortion in the Fermi surface is due to the small misalignment of the analyser corresponds to the normal emission of photoelectrons from sample.

Experimental data presented in Figs. 2 and 3 unveil the detailed electronic structure of YPtBi. Figure 2a shows the Fermi surface map revealing the presence of multiple Fermi pockets including two circular-like Fermi pockets around the Γ point and six half oval-shaped pockets around the K points of the BZ. Figure 2b presents the zoomed in plot along the K–M–K high symmetry direction and clearly shows the complex half oval-like Fermi pockets. Figure 2c shows the constant energy contour plot at the binding energy of 250 meV, where the circular-like Fermi pocket at the Fermi surface around zone centre point evolves into a twin hexagonal shape. This feature is a consequence of the possible spin-splitting, commonly seen on the surface of the non-centrosymmetric metallic compounds. Furthermore, a small circular feature evolves at the zone centre point as a result of metallic band crossings. Figure 2d shows a constant energy contour in the vicinity of the Dirac point (binding energy \sim 500 meV) in which we observe the circular-shaped feature splitting into two concentric circles. In order to reveal the nature of the Fermi pockets, constant energy contour plots at various binding energies are taken and stacked into an energy versus momentum plot in Fig. 2e. By moving towards the higher binding energy, we observe that the circular-like pocket at the zone centre increases in size and resembles a perfect hexagonal shape. This confirms both the hole-like and hexagonal nature of the pocket. Additionally, the oval-like shape around the K point shrinks into a point and a small circular feature evolves at the zone centre around 250 meV. This confirms the electron-like nature of the Fermi pockets at the K point of the BZ. At the Fermi level we observe a line-like feature crossing M points and connecting the two consecutive BZs as well as separating the two oval-like pockets. However, as we move towards higher binding energies it is observed that the line gap increases and evolves into two distinct segments breaking the outer circle around the Γ point. The special outer circle located at around 100 meV below the Fermi level could potentially represent another pair of Kramers points²⁸.

In order to reveal the nature of the bands, we present in Fig. 3 the dispersion map along the M– Γ –M direction in which we observe hole-like bands and electron-like bands crossing the Fermi level near the Γ point and near the M point, respectively. Interestingly, we observe a Dirac state at the Γ point at 500 meV below the Fermi level. Furthermore, we observe another surface state at around 250 meV below the Fermi level. Figure 3b,c presents the second derivative plot using curvature method³⁴, where the Dirac point is clearly visible. In order to reveal the origin of the bands, slab calculations were performed which are presented in Fig. 3d. Here, it is clearly observed that the electron-like bands cross the Fermi level. Furthermore, we observe the Rashba-split states in the vicinity of the Fermi level around the M point. The surface calculations (see Fig. 4a) confirm the surface nature of Rashba-split states and the existence of electron-like band at the M-point.

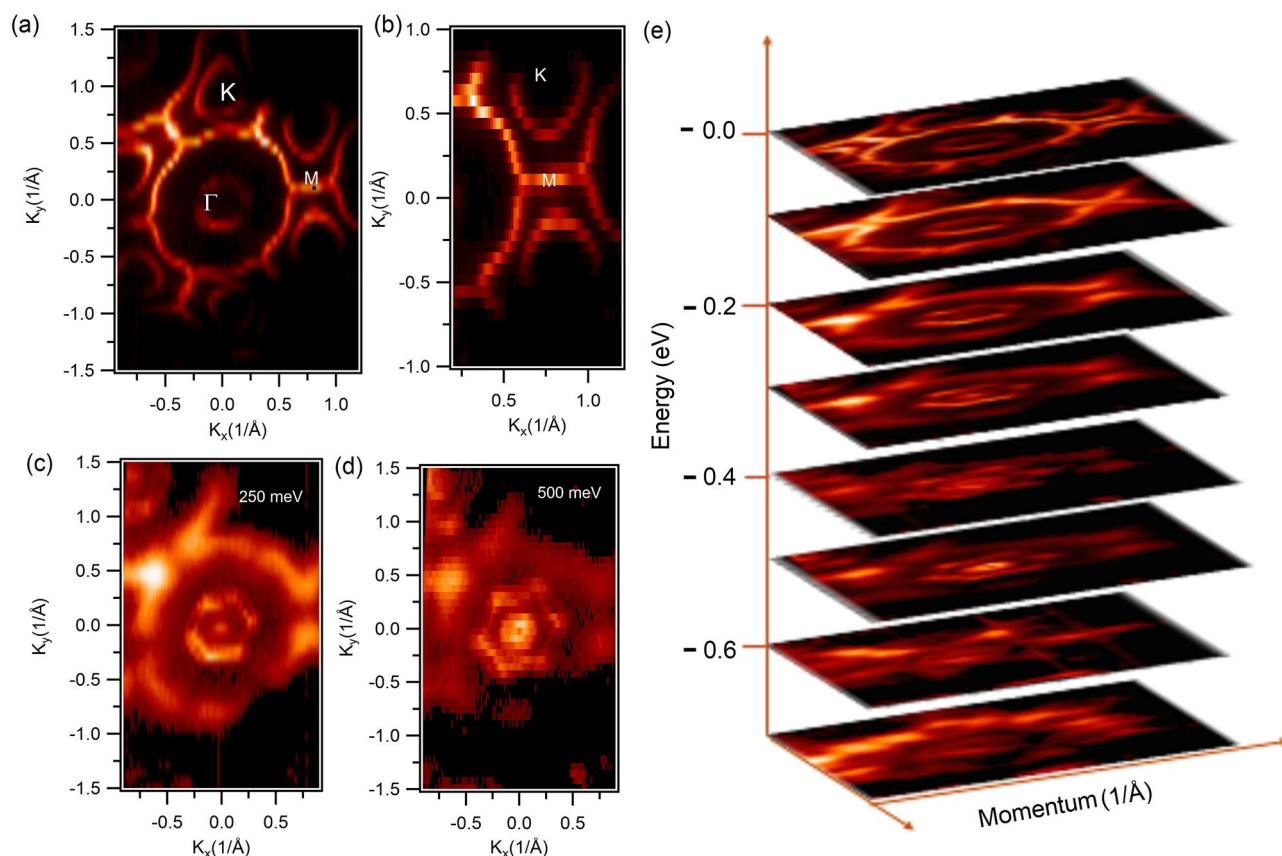


Figure 2. Fermi surface map of YPtBi. (a) Fermi surface map at a photon energy of 60 eV. High symmetry points are marked in the plot. (b) Zoomed in plot of Fermi surface along the K–M–K direction. (c,d) Constant energy contour plots at binding energies of 250 meV and 500 meV, respectively. (e) Constant energy contour plots stacked in order to show the form of the bands (zero energy corresponds to the Fermi level).

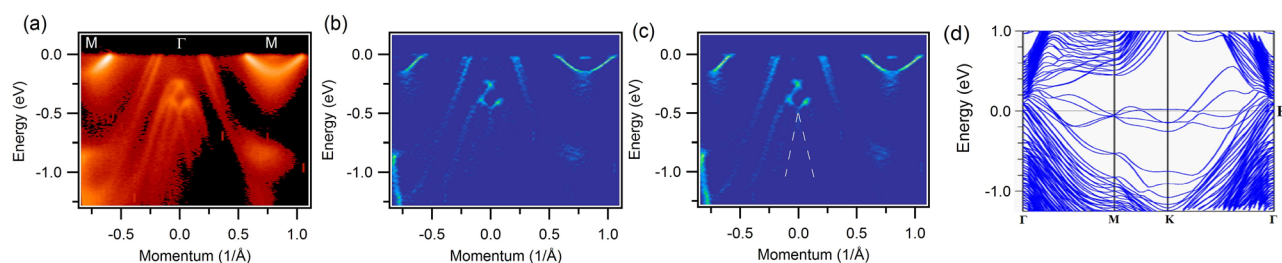


Figure 3. Observation of Dirac state in YPtBi. (a) Measured dispersion map along the M– Γ –M direction at a photon energy of 60 eV. (b,c) Second derivative plot of (a) using the curvature method. White dashed line denoting Dirac state in figure (c) serves as a guide for the eyes. (d) Theoretical energy dispersion map along the Γ –M–K– Γ high symmetry direction.

Here, we discuss the results of our first-principles calculations which are presented in Fig. 4. Figure 4a shows the results of calculations of electronic structure for the Bi-terminated surface, with the inclusion of spin-orbit coupling, along the M– Γ –M direction. The red highlighted bands represent the surface bands. The calculations agree well with our experimental results which show the Dirac point located at around 500 meV below the Fermi level. Furthermore, it shows the Rashba-split band and the electron-like band around the M point. The energy location of the other surface state at the Γ point is slightly mismatched with our experimentally observed energy location. Since these bands are the metallic surface state defined within the 2D surface, the position of the surface state might be controlled by impurity potential at the surface. This type of energy mismatching has also been reported earlier²⁶. The relative energy shift (~ 300 meV) between ARPES data and predicted band calculations has been previously reported and is potentially due to the charge imbalance of the cleaved surface (see Ref.³¹). Moreover, electron-like band along the Γ –M direction is confirmed as surface-originated. Figure 4b displays the first-principles calculations of electronic structure for the Bi-terminated surface without the inclusion of SOC, which does not show a Dirac-like state. We conclude that the linear Dirac bands originate from the spin-orbit

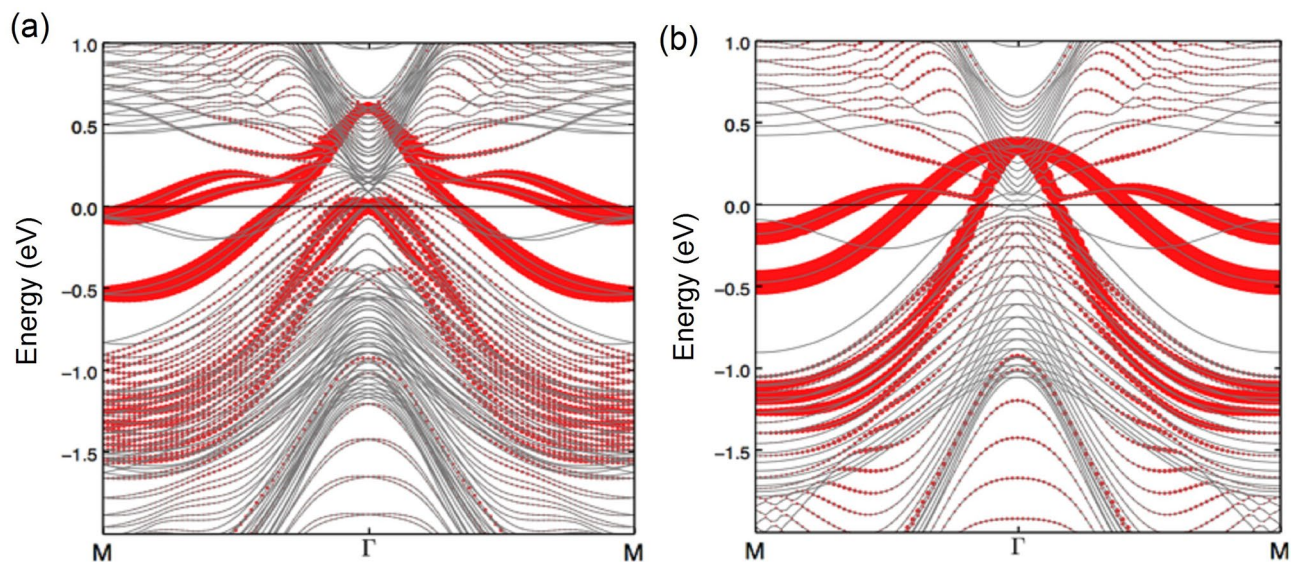


Figure 4. First-principles calculations of Bi-terminated surface state of YPtBi. Electronic band structure of YPtBi along the M– Γ –M direction **(a)** with inclusion of spin-orbit coupling (SOC) and **(b)** without inclusion of SOC. The red highlight indicates the surface states. The red dots represent the presence of the surface state (Bi atoms at the surface in the slab geometry). The size of red dots shows how much the surface atom is contained in each eigenstate in the band structure. In other words, the larger red circle indicates the more surface atom character contained in the given quasiparticle state.

coupling arising from heavy Bi atom. The possibility of being Rashba split state or quantum subbands can be ruled out. If it is merely another pair of Rashba split, one would expect two counter propagating states, which is not observed in both our experimental and calculated band structure. Furthermore, such a large Rashba splitting with required Rashba parameter value $\alpha_R \sim 2.9 \text{ eV\AA}$ is not expected just by the two-dimensional electronic confinement within the surface band-bending or by the potential gradient arising from the band bending near the Fermi surface.

Discussion

Considering the experimental and theoretical study of half-Heusler compound YPtBi, both confer the same information regarding the location of the Dirac points at around 500 meV below the Fermi level at the Γ point. At this high symmetry point, we notice that the Dirac state originates from the surface which is the result of the strong SOC. Our data qualitatively agree with the study of Liu et al.²⁶, however, we do not observe any intrinsic global band gap in YPtBi, which is essential for material to be a topological insulator. This is in accord with the results of our previous studies of specific heat and electrical resistivity, which indicate the semimetallic character of YPtBi³². Therefore, we attribute such linearly dispersive band to a Dirac state instead of topological surface state. Moreover, our experimental measurements as well as calculations reveal possible Rashba-split states in the vicinity of Fermi surface at the M point due to an antisymmetric spin-orbit coupling created by the electric field gradient as a consequence of non-centrosymmetric crystal structure.

Conclusions

In conclusion, we have performed ARPES measurements on the ternary superconducting half-Heusler compound YPtBi in its normal state. Our data reveal the presence of multiple Fermi pockets at the Fermi surface of YPtBi. Furthermore, we directly observe the Dirac state at 500 meV below the Fermi level at the Γ point of the BZ. We further observe multiple surface states in our Fermi surface maps. Our first-principles calculations reveal a Rashba-split feature at the M point. We believe that results of our study will stimulate the research interest in investigation of other compounds from half-Heusler family which are possible topological materials.

Methods

The single crystals of YPtBi were grown from Bi flux as described in Ref.³². The chemical composition of YPtBi was checked by energy-dispersive X-ray analysis using a FEI scanning electron microscope equipped with an EDAX Genesis XM4 spectrometer. Homogeneous single-phase materials with their stoichiometry close to equiatomic were observed. Crystal structure of our sample was studied by means of X-ray diffraction on powdered single crystals using an X'pert Pro PAN analytical diffractometer with Cu-K α radiation. It was confirmed that YPtBi crystallises in a space group $F\bar{4}3m$ with lattice parameter $a = 6.65(1)\text{\AA}$, which is in a perfect agreement with previously reported data²⁹. The synchrotron based experiments were performed at the ALS BL 10.0.1 equipped with R4000 hemispherical electron analyser at temperature of 15 K. For the synchrotron measurement the energy resolution was set to better than 20 meV and the angular resolution was set to better than 0.2° . The electronic structure calculations were carried out using the full-potential linearised augmented plane

wave (FP-LAPW) method implemented in the WIEN2k package³⁵, and the PBEsol was used as the exchange-correlation functional³⁶. In order to simulate surface effects along the (111) surface, we constructed the hexagonal unit cell of 3 formula units with c-axis along (111) surface. Then we built the $1 \times 1 \times 6$ supercell for the (111) surface, with a vacuum thickness of 20 Å. The spin-orbit coupling was considered with the perturbation in the electronic structure calculations.

Data availability

The datasets analysed during the current study are available from the corresponding author on reasonable request.

Received: 2 March 2020; Accepted: 9 July 2020

Published online: 23 July 2020

References

- Hasan, M. Z. & Kane, C. L. Colloquium: Topological insulators. *Rev. Mod. Phys.* **82**, 3045–3067 (2010).
- Qi, X. L. & Zhang, S. C. Topological insulators and superconductors. *Rev. Mod. Phys.* **83**, 1057–1110 (2011).
- Xia, Y. *et al.* Observation of a large-gap topological-insulator class with a single Dirac cone on the surface. *Nat. Phys.* **5**, 398–402 (2009).
- Bansil, A., Lin, H. & Das, T. Colloquium: Topological band theory. *Rev. Mod. Phys.* **88**, 021004 (2016).
- Wang, Z., Weng, H., Wu, Q., Dai, X. & Fang, Z. Three-dimensional Dirac semimetal and quantum transport in Cd₃As₂. *Phys. Rev. B* **88**, 125427 (2013).
- Neupane, M. *et al.* Observation of a three-dimensional topological Dirac semimetal phase in high-mobility Cd₃As₂. *Nat. Commun.* **5**, 3786 (2014).
- Fu, L. Topological crystalline insulators. *Phys. Rev. Lett.* **106**, 106802 (2011).
- Xu, Q. *et al.* Two-dimensional oxide topological insulator with iron-pnictide superconductor LiFeAs structure. *Phys. Rev. B* **92**, 205310 (2015).
- Neupane, M. *et al.* Surface electronic structure of the topological Kondo-insulator candidate correlated electron system SmB₆. *Nat. Commun.* **4**, 2991 (2013).
- Yang, B. J. & Nagaosa, N. Classification of stable three-dimensional Dirac semimetals with nontrivial topology. *Nat. Commun.* **5**, 4898 (2014).
- Neupane, M. *et al.* Observation of the spin-polarized surface state in a noncentrosymmetric superconductor BiPd. *Nat. Commun.* **7**, 13315 (2016).
- Young, S. M. & Kane, C. L. Dirac semimetals in two dimensions. *Phys. Rev. Lett.* **115**, 126803 (2015).
- Huang, S. M. *et al.* A Weyl Fermion semimetal with surface Fermi arcs in the transition metal monopnictide TaAs class. *Nat. Commun.* **6**, 7373 (2015).
- Weng, H., Fang, C., Fang, Z., Bernevig, B. A. & Dai, X. Weyl semimetal phase in noncentrosymmetric transition-metal monophosphides. *Phys. Rev. X* **5**, 011029 (2015).
- Xu, S. Y. *et al.* Discovery of a Weyl fermion semimetal and topological Fermi arcs. *Science* **349**, 613 (2015).
- Lv, B. Q. *et al.* Experimental discovery of Weyl semimetal TaAs. *Phys. Rev. X* **5**, 031013 (2015).
- Neupane, M. *et al.* Observation of topological nodal Fermion semimetal phase in ZrSiS. *Phys. Rev. B* **93**, 201104 (2016).
- Chadov, S. *et al.* Tunable multifunctional topological insulators in ternary Heusler compounds. *Nat. Mater.* **9**, 541 (2010).
- Lin, H. *et al.* Half-Heusler ternary compounds as new multifunctional experimental platforms for topological quantum phenomena. *Nat. Mater.* **9**, 546 (2010).
- Al-Sawai, W. *et al.* Topological electronic structure in half-Heusler topological insulators. *Phys. Rev. B* **82**, 125208 (2010).
- Wan, X., Turner, A. M., Vishwanath, A. & Savrasov, S. Y. Topological semimetal and Fermi-arc surface states in the electronic structure of pyrochlore iridates. *Phys. Rev. B* **83**, 205101 (2011).
- Ruan, J. *et al.* Symmetry-protected ideal Weyl semimetal in HgTe-class materials. *Nat. Commun.* **7**, 11136 (2016).
- Pavlosiuk, O., Kaczorowski, D., Fabreges, X., Gukasov, A. & Wiśniewski, P. Antiferromagnetism and superconductivity in the half-Heusler semimetal HoPdBi. *Sci. Rep.* **6**, 18797 (2016).
- Nakajima, Y. *et al.* Topological RPDBi half-Heusler semimetals: A new family of noncentrosymmetric magnetic superconductors. *Sci. Adv.* **1**, e1500242 (2015).
- Hirschberger, M. *et al.* The chiral anomaly and thermopower of Weyl fermions in the half-Heusler GdPtBi. *Nat. Mater.* **15**, 1161 (2016).
- Liu, Z. K. *et al.* Observation of unusual topological surface states in half-Heusler compounds LnPtBi (Ln = Lu, Y). *Nat. Commun.* **7**, 12924 (2016).
- Logan, J. A. *et al.* Observation of a topologically non-trivial surface state in half-Heusler PtLuSb (001) thin films. *Nat. Commun.* **7**, 11993 (2016).
- Liu, C. *et al.* Metallic surface electronic state in half-Heusler compounds RPtBi (R = Lu, Dy, Gd). *Phys. Rev. B* **83**, 205133 (2011).
- Butch, N. P., Syers, P., Kirshenbaum, K., Hope, A. P. & Paglione, J. Superconductivity in the topological semimetal YPtBi. *Phys. Rev. B* **84**, 220504 (2011).
- Bay, T. V. *et al.* Low field magnetic response of the non-centrosymmetric superconductor YPtBi. *Sol. Stat. Commun.* **13**, 183 (2014).
- Kim, H. *et al.* Beyond triplet: Unconventional superconductivity in a spin-3/2 topological semimetal. *Sci. Adv.* **4**, eaao4513 (2018).
- Pavlosiuk, O., Kaczorowski, D. & Wiśniewski, P. Superconductivity and Shubnikov–de Haas oscillations in the noncentrosymmetric half-Heusler compound YPtBi. *Phys. Rev. B* **94**, 035130 (2016).
- Nowak, B. & Kaczorowski, D. NMR as a probe of band inversion in topologically nontrivial half-Heusler compounds. *J. Phys. Chem. C* **118**, 18021–18026 (2014).
- Zhang, P. *et al.* A precise method for visualizing dispersive features in image plots. *Rev. Sci. Instrum.* **82**, 043712 (2011).
- Blaha, P., Schwarz, K., Madsen, G. K. H., Kvasnicka, D. & Luitz, J. *WIEN2K, an augmented plane wave + local orbitals program for calculating crystal properties* (Karlheinz Schwarz Techn. Universität Wien, Wien, 2001).
- Perdew, J. P. *et al.* Restoring the density-gradient expansion for exchange in solids and surfaces. *Phys. Rev. Lett.* **100**, 136406 (2008).

Acknowledgements

M.N. is supported by the Air Force office of Scientific Research under Award No. FA9550-17-1-0415 and the Center for Thermal Energy Transport under Irradiation, an Energy Frontier Research Center funded by the U.S. DOE, office of Basic Energy Sciences. T.D. is supported by NSF IR/D program. O.P., P.W. and D.K. are supported by the National Science Centre (Poland) under research grant 2015/18/A/ST3/00057. O.P. is supported by the Foundation for Polish Science (FNP), program START 66.2020. Work at Los Alamos National Laboratory (LANL) is supported by U.S. DOE Contract No. DE-AC52-06NA25396 through the LANL LDRD Program (H.C.

and J.-X.Z.). This work was, in part, supported by the Center for Integrated Nanotechnologies, a U.S. DOE BES user facility, in partnership with the LANL Institutional Computing Program for computational resources. This research used resources of the Advanced Light Source, a U.S. DOE Office of Science User Facility, under Contract No. DE-AC02-05CH11231. We also thank Sung-Kwan Mo for beamline assistance at the LBNL.

Author contributions

M.N. and D.K. conceived the study; P.W. and O.P. synthesized the single crystals and performed their structural characterization; M.M.H. and M.N. performed the ARPES measurements and analysed obtained data with the help of G.D., K.D., F.K., T.D. and C.S.; M.M.H. and M.N. wrote the manuscript with input from all authors; H.C. and J.-X.Z. carried out the electronic structure calculations; M.N. was responsible for the overall research direction, planning and integration among different research units.

Competing interests

The authors declare no competing interests.

Additional information

Correspondence and requests for materials should be addressed to O.P. or M.N.

Reprints and permissions information is available at www.nature.com/reprints.

Publisher's note Springer Nature remains neutral with regard to jurisdictional claims in published maps and institutional affiliations.



Open Access This article is licensed under a Creative Commons Attribution 4.0 International License, which permits use, sharing, adaptation, distribution and reproduction in any medium or format, as long as you give appropriate credit to the original author(s) and the source, provide a link to the Creative Commons license, and indicate if changes were made. The images or other third party material in this article are included in the article's Creative Commons license, unless indicated otherwise in a credit line to the material. If material is not included in the article's Creative Commons license and your intended use is not permitted by statutory regulation or exceeds the permitted use, you will need to obtain permission directly from the copyright holder. To view a copy of this license, visit <http://creativecommons.org/licenses/by/4.0/>.

© The Author(s) 2020